Impact of Scattering within a Multipath Simulator Antenna Array on the Ricean Fading Distribution Parameters in OTA Testing

Andrés Alayón Glazunov, *Senior Member, IEEE*, Sathyaveer Prasad, Peter Händel, *Senior Member, IEEE*, Thomas Bolin, Kjell Prytz

***Abstract*—In this paper we investigate the unwanted scattering that exists within the MultiPath Simulator (MPS) array antennas employed in Over The Air (OTA) testing of mobile terminals. The impact of scattering is evaluated in terms of the measurement uncertainty of the average received power and the Ricean $K-$factor. The maximum ratio combining diversity is investigated for a generic device under test comprising two half-wavelength dipole antennas. We provide closed-form expressions for the uncertainties of the average received power and the Ricean $K-$factor for a uniform circular array of MPS antennas and a 2D uniformly distributed angle-of-arrival spectrum. We also derive the maximum number of MPS antennas and the minimum ring radius of the MPS system as a function of the separation between the most distant antenna elements if the device under test employs a uniform linear array. As a result, we provide design guidelines for MPS array in terms of the number antennas, the radius of the MPS array and the wavelength of the carrier frequency.**

***Index Terms*—Multipath simulator, scattering, measurement accuracy, Ricean $K-$factor, maximum ratio combining diversity.**

I. Introduction

Multiple Input Multiple Output (MIMO) techniques have become key performance boosters in new wireless technologies such as the Long Term Evolution (LTE), LTE-Advanced and mobile Worldwide Interoperability for Microwave Access (WiMAX) standards, [1]. MIMO antenna systems employ antennas with multiple elements at both sides of the communication link. Hence, a satisfactory performance of MIMO systems entails a satisfactory performance of the antennas too. The role of the antennas has now become even more critical as compared to their role in Single Input Single Output (SISO) systems, which employ one receive antenna and one transmit antenna. Previously, the focus had been on figures of merit that did not take into account the propagation channel. However, it is no longer possible to neglect the propagation channel while testing MIMO antenna systems, since the overall performance depends upon the statistical properties of the propagation channel and its interaction with the antennas.

Over-the-air (OTA) testing has become the standard approach for measuring the radiated performance of mobile terminals in SISO systems, [2, 3]. SISO and MIMO OTA testing have been extensively researched over more than a decade. Standardization efforts in the CTIA and the 3GPP have been supported by contributions from both industry and academia. An especially fruitful forum has been developed within several COST (COoperation in Science and Technology) Actions supporting cooperation among scientists and researchers across Europe. Currently, the ongoing COST Action IC1004 has a working group pursuing MIMO OTA testing research, [4]. The ultimate goal with this research is to contribute the homologation, by the standardisation bodies, of one or several OTA testing techniques capable of differentiating MIMO devices with good performance from devices with bad performance in a reliable, efficient and cost-effective manner.

MIMO OTA testing techniques can be roughly divided into two main groups depending on the type of measurement chamber used: *anechoic* chamber techniques and *reverberation* chamber techniques [5]. They take fundamentally different approaches for generating a fading propagation channel. In anechoic chambers, arbitrary field distributions can be generated without disturbance from the walls in the desired directions of the Angle of Arrival (AoA). On the other hand, in reverberation chambers, the walls are highly reflective (metallic) and the resulting field is an isotropically distributed fading field. For a more complete account of the different techniques and their variations, see [5–8] and the references therein. Comparisons of the different techniques can also be found there.

In this paper we focus on the MPS technique, which is an anechoic chamber OTA testing technique. An MPS consists of an array of antennas (also known as multiprobe system) surrounding the device under test (DUT) at a distance of few wavelengths, [9–11]. A feed network which distributes the signals over the array is used to apply different amplitudes and varying phase shifts at the array antennas. In this way several waves are generated out of the MPS antennas which upon superposition at the DUT simulate a multipath fading environment. A schematic representation of a Uniform Circular Array (UCA) of MPS antennas is shown in Fig. 1.

Accuracy is key in evaluating the performance of a DUT, therefore we need to evaluate the measurement uncertainty due to various sources of error. In this paper, we focus on the unwanted scattering that exists within the MPS array antennas, i.e., the interference signals that arise within the antenna arrays themselves. Various research papers have been published on the MPS technique highlighting different aspects of measurements and the impact of various parameters on the measurement uncertainty. For example, in [11], an experimental UCA MPS system was built and evaluated at frequencies $2-2.6$ GHz. In addition to showing the feasibility of the MPS

method, another main conclusion was that 16 MPS antennas ought to be used to generate stable fading signal statistics. Further, a rule of thumb for the number of single polarized OTA antennas required to achieve a certain uncertainty level of the field at the test zone was given by (3) in [12]. In [13], it is shown that in order to achieve field strength and phase stability across the test zone the ratio between the radius of a test zone and the radius of a ring of OTA antennas has to be $1/10$ or lower in the frequency range $0.5-6$ GHz. The impact of scattering within an MPS array on the measurement uncertainty of the MPS system was first studied in [14]. An expression is derived for the standard deviation of the average received power in a Rayleigh fading environment. As a result of simulations and measurements it is suggested that for MPS antennas in the range $8-16$ and MPS ring radius in the range of $1-2$ m the measurement uncertainty could be within $\pm(0.1-1)$ dB. However, in spite of the contributions on the topic there are still plenty of issues to be analyzed. For example, the impact of scattering within the MPS antennas on the fading statistics of the emulated propagation channel has not been studied previously. In this paper we present a remedy to this situation by filling the gap:

- We derive the maximum number of MPS antennas and the minimum ring radius of the MPS system as a function of the separation between the most distant antenna elements if the DUT employs a Uniform Linear Array (ULA). The far-field condition employed is based on a distance criterium for the antenna gain correction factor to Friis equation [15].
- We provide closed-form expressions for the uncertainties of the average received power and the Ricean $K-$factor for a UCA of MPS antennas and a 2D uniformly distributed AoA spectrum.
- We investigate the Maximum Ratio Combining (MRC) diversity for a generic DUT comprising two half-wavelength dipole antennas.
- We provide system emulation guidelines for MPS array in terms of the number of MPS antennas, the radius of the MPS array, the physical size of the DUT and the carrier frequency.
- We present experimental data to validate our numerical findings.

II. MPS Scattering Signal Model

In our analysis we consider a UCA of radius R consisting of N_{MPS} MPS antennas surrounding N_{DUT} DUT antennas shown in Fig. 1. We make the following assumptions on the MPS antennas to enable our modeling approach:

1) Each element of the MPS array is matched, which means that there is no power reflected back from the antenna load due to mismatch. Hence, the scattered power depends only on the physical properties of the antenna aperture, i.e., its shape, size and material.
2) The elements of the MPS array are $\lambda/2$-dipoles, which are minimum scattering antennas. Hence, the scattered power is equal in magnitude to the received power and the scattered field pattern is equal to the radiation pattern of the antenna.

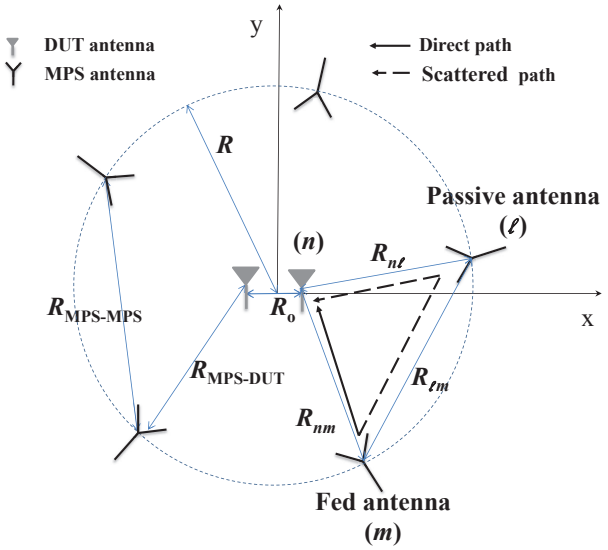

Fig. 1: Arrangement of antennas in two-antenna DUT MPS system as uniform circular array and showing the direct and scattered paths from the fed MPS antenna to DUT antennas.

Now assume that MPS antenna m is fed, while all the other MPS antennas $\ell \neq m$ will act as passive scatterers. Hence, the total voltage induced at the DUT antenna port n is comprised by two terms

$$v_{n,m}^{\mathrm{total}} = v_{n,m}^{\mathrm{direct}} + v_{n,m}^{\mathrm{indirect}}, \tag{1}$$

where $v_{n,m}^{\mathrm{direct}}$ is the voltage induced by the wave incoming directly from the fed MPS antenna m and

$$v_{n,m}^{\mathrm{indirect}} = \sum_{\substack{\ell=1 \\ \ell\neq m}}^{N_{\mathrm{MPS}}} v_{n,\ell,m}^{\mathrm{indirect}}, \tag{2}$$

is the voltage induced by the wave also originated at the fed MPS antenna m, but arriving at the DUT due to scattering from MPS antennas $\ell \neq m$ under the assumption that there is only single scattering. Single scattering means here that only the first "signal bounce" from the scattering MPS antenna is considered. In reality this signal propagates further and is scattered anew by another MPS antenna and so far and so on giving place to infinite multiple bounces; they, however, can be neglected due to additional path loss. In order to obtain the induced voltages we follow the approach outlined in [16]; however, without taking into account multiple scattering.

The voltage associated with the direct signal $v_{n,m}^{\mathrm{direct}}$ is obtained as a function of the power received at DUT n and coming from the fed MPS antenna m, which is given by the Friis transmission formula [17]

$$P_{n,m}^{\mathrm{direct}} = P_m G_m G_n \eta_{n,m} \left(\frac{\lambda}{4\pi R_{n,m}}\right)^2, \tag{3}$$

where P_m is the total radiated power by MPS antenna m, $R_{n,m}$ is the distance between DUT antenna n and MPS antenna m as shown in Fig.1, G_m and G_n are the corresponding antenna gains evaluated along the line given by $R_{n,m}$, $\eta_{n,m}$ is

the polarization mismatch between the two antennas. Hence, the corresponding induced voltage is given by

$$v_{n,m}^{\text{direct}} = c\sqrt{P_{n,m}^{\text{direct}}}\mathrm{e}^{-j(kR_{n,m}+\psi_{n,m})}, \tag{4}$$

where c and $\psi_{n,m}$ are a proportionality constant and the random phase shifts respectively, both related to the receive DUT antenna n, $kR_{n,m}$ accounts for the phase delay of the signal going from transmitter to receiver, i.e., from MPS antenna m to DUT antenna n.

The voltage associated with the indirect signal $v_{n,m}^{\text{indirect}}$ is then obtained with the help of the two assumptions listed above. Thus, the power scattered (reradiated) by MPS antenna ℓ originated at the MPS antenna m is obtained by applying Friis transmission formulas to the corresponding antennas

$$P_{\ell,m} = P_m G'_m G'_\ell \eta_{\ell,m}\left(\frac{\lambda}{4\pi R_{\ell,m}}\right)^2, \tag{5}$$

where $R_{\ell,m}$ is the distance between MPS antenna ℓ and MPS antenna m, G'_m and G'_ℓ are the corresponding antenna gains evaluated along the line given by $R_{\ell,m}$. Hence, the indirect received power can be written as follows

$$P_{n,\ell,m}^{\text{indirect}} = P_{\ell,m} G_n G_\ell \eta_{n,\ell}\left(\frac{\lambda}{4\pi R_{n,\ell}}\right)^2. \tag{6}$$

The corresponding induced voltage is then modeled as

$$v_{n,m}^{\text{indirect}} = c\sum_{\substack{\ell=1\\ \ell\neq m}}^{N_{\text{MPS}}}\sqrt{P_{n,\ell,m}^{\text{indirect}}}\mathrm{e}^{-j(k(R_{n,\ell}+R_{\ell,m})+\psi_{n,\ell,m})}, \tag{7}$$

where c is a constant related to the receive DUT antenna n, and $\psi_{n,\ell,m}$ is related to both the DUT and MPS antennas, $k(R_{n,\ell}+R_{\ell,m})$ accounts for the phase delay of the signal going from MPS antenna m, to MPS antenna ℓ and finally to DUT antenna n (see Fig. 1).

The total voltage induced at DUT antenna n and coming both directly or indirectly is obtained from (1) and (3)-(7)

$$v_n^{\text{total}} = \sum_{m=1}^{N_{\text{MPS}}} v_{n,m}^{\text{total}} = v_n^{\text{direct}} + v_n^{\text{indirect}}, \tag{8}$$

where the desired signal, i.e., the direct signal (4)

$$v_n^{\text{direct}} = \sum_{m=1}^{N_{\text{MPS}}} v_{n,m}^{\text{direct}}, \tag{9}$$

will be corrupted by the scattering within the MPS antenna array given by the indirect signal (7)

$$v_n^{\text{indirect}} = \sum_{m=1}^{N_{\text{MPS}}} v_{n,m}^{\text{indirect}}. \tag{10}$$

The model we have derived above is simple yet useful since it is based on quantities such as the antenna gain, transmit power and it can be directly simulated from any given geometry. It can be easily extended to other than the UCA MPS configuration.

III. Farfield Conditions for MPS design

Let us assume that all the MPS antennas are identical and located in the far-field of each other which justifies the use of Friis equation in the previous section. In this paper we use the quadratic antenna gain reduction factor criterium for low-gain antennas to define the far-field distance R_{ref} between two identical antennas at boresight [15]

$$R_{\text{ref}} = \frac{4\lambda G}{\pi^2}\sqrt{\frac{\alpha_{\text{E}}}{1-\gamma_{\text{A}}}}, \tag{11}$$

where λ is the wavelength, G is the antenna gain, $\alpha_{\text{E}} = 0.06$ is a fitting coefficient that is the same for all antennas and γ_{A} is the antenna gain reduction factor. Hence, by choosing γ_{A} we can straightforwardly obtain the starting point of the corresponding far-field region for a required error magnitude of the antenna gain defined by $1-\gamma_{\text{A}}$. An errorless assumption of the antenna gain in the Friis equations, such that $\gamma_{\text{A}} \to 1$ requires the antennas to be at an infinite distance from each other, i.e., $R \to \infty$, independently of the antenna gain or the wavelength. In [15] the shortest distance for reliable performance of the correction to Friis equation is given for various antennas. Here, we specialize to dipole like antennas and therefore we choose the $\lambda/2$–dipole to evaluate the far-field distance with gain $G = 1.64$. In this case the shortest reliable distance equals 0.35λ with corresponding correction factor $\gamma_{\text{A}} = 0.7862$. Hence, the correction factor can be chosen within the interval $0.7862 \leq \gamma_{\text{A}} < 1$ with corresponding normalized antenna separation within the interval $0.35 \leq R_{\text{ref}}/\lambda < \infty$. Since our objective is to use the Friis equations we choose $\gamma_{\text{A}} = 0.99$ such that the introduced antenna error of 1% is much smaller than the error magnitudes tolerable in OTA testing [3]. Hence, specializing our analysis to $\lambda/2$-dipoles we can insert $\gamma_{\text{A}} = 0.99$ and $G = 1.64$ into (11) to obtain a reference distance defining the start of the far-field zone, $R_{\text{ref}} \approx 1.63\lambda$. More practical antennas employed in wireless devices have $G = 1$, which give $R_{\text{ref}} \approx 0.99\lambda$.

The distance between any two adjacent MPS antennas in the array $R_{\text{MPS-MPS}}$ shall satisfy the following distance criterium for the far-field zone at a fixed value of the antenna gain reduction factor γ_{A}

$$R_{\text{MPS-MPS}} \geq R_{\text{ref}}, \tag{12}$$

where R_{ref} is given by (11). Following the geometry given in Fig. 1, the distance between any two adjacent MPS array antennas can be written as follows

$$R_{\text{MPS-MPS}} = 2R\sin\left(\frac{\pi}{N_{\text{MPS}}}\right). \tag{13}$$

Under the assumption that both the DUT and MPS antennas are in the far-field of each other, i.e. at distances grater than (11), the distance between the DUT and MPS antennas needs to satisfy

$$R_{\text{MPS-DUT}} \geq R_{\text{ref}}. \tag{14}$$

Now, further assuming that the DUT antennas are identical, we denote the shortest distance between a DUT antenna and an MPS antenna as follows

$$R_{\text{MPS-DUT}}^{\text{shortest}} = R - \frac{R_o}{2}, \tag{15}$$

TABLE I: Minimum MPS ring radius R/λ and corresponding number of MPS antennas N_{MPS} for a given separation distance between DUT antennas R_o for antenna gains $G = 1.64$ and $G = 1$ with correction factor $\gamma_{\mathrm{A}} = 0.99$.

R_o/λ	0.1	0.2	0.3	0.4	0.5	0.6	0.7	0.8	0.9	1
$G = 1.64(2.15$ dBi$)$										
R^{m}/λ	1.68	1.73	1.78	1.83	1.88	1.93	1.98	2.03	2.08	2.13
$N^{\mathrm{m}}_{\mathrm{MPS}}$	6	6	6	6	7	7	7	7	7	8
$G = 1(0$ dBi$)$										
R^{m}/λ	1.04	1.09	1.14	1.19	1.24	1.29	1.34	1.39	1.44	1.49
$N^{\mathrm{m}}_{\mathrm{MPS}}$	6	6	6	7	7	7	8	8	8	9

where R_o is the separation distance between the DUTs and R is the radius of the MPS array for which it is valid that $R^{\mathrm{shortest}}_{\mathrm{MPS-DUT}} \leq R_{\mathrm{MPS-DUT}}$.

Now using (12)-(15) we obtain the condition to be satisfied by the ring radius R given R_{ref}, R_o and N_{MPS}

$$R \geq \max\left(\frac{R_{\mathrm{ref}}}{2\sin\left(\frac{\pi}{N_{\mathrm{MPS}}}\right)}, R_{\mathrm{ref}} + \frac{R_o}{2}\right), \tag{16}$$

where the function $\max(a, b)$ equals the largest of a and b.

The smallest ring radius is obtained when the arguments in (16) are equal, i.e., $\min\max(a, b) = a = b$. In our case this gives the equation

$$\frac{R_{\mathrm{ref}}}{2\sin\left(\frac{\pi}{N_{\mathrm{MPS}}}\right)} = R_{\mathrm{ref}} + \frac{R_o}{2}, \tag{17}$$

Given R_o and R_{ref} we obtain the corresponding number of MPS antennas

$$N^{\mathrm{m}}_{\mathrm{MPS}} = \left\lfloor \frac{\pi}{\arcsin\left(\frac{R_{\mathrm{ref}}}{2R_{\mathrm{ref}}+R_o}\right)} \right\rfloor, \tag{18}$$

where the function $\lfloor c \rfloor$ maps a real number c to the largest previous integer number. The minimum normalized ring radius is then given by

$$\frac{R^{\mathrm{m}}}{\lambda} = \frac{R_{\mathrm{ref}}}{\lambda} + \frac{R_o}{2\lambda}, \tag{19}$$

Table I shows the the minimum MPS ring radius and the corresponding number of MPS antennas for different values of the normalized maximum separation distance between the DUT antennas R_o obtained using (18) and (19), respectively.

Hence, in order to design an MPS system where all involved antennas are in the far-field region of each other, the above limitations on the MPS ring radius and the number of MPS antennas can be used. It is worthwhile to mention that in this case, the limitations on the number of MPS antennas and the size of the quite zone to achieve a given accuracy level of the reproduced field presented in [12] and [13] are both fulfilled too. Moreover, the found relationships may serve as a guideline for designing MPS arrays that are compact in size; hence allowing for miniaturization alternatives. In addition to that, the relationships can be used to evaluate upper bounds on uncertainties since they give the maximum number of MPS antennas for a given size of the DUT array.

IV. Channel Fading Accuracy Evaluation

The measurement uncertainty of the MPS system is evaluated by introducing uncertainty measures for the propagation channel parameters for a given Ricean channel and also in terms of MRC diversity.

A. Ricean Fading Statistics

In order to study the impact of scattering on the accuracy of the emulated propagation channel we assume the desired channel behavior to be described by the Ricean probability density function (pdf). Hence, if a test antenna (let's say a $\lambda/2$-dipole) is placed at the center of the UCA MPS antenna system then the probability density of the magnitude of the complex signal received by the antenna $|v|$ is given by, [18]

$$f_{|v|}(|v|) = \frac{2(1+K)|v|}{P_{\mathrm{rec}}} \exp\left(-K - \frac{(K+1)|v|^2}{P_{\mathrm{rec}}}\right) \times I_0\left(2\sqrt{\frac{K(1+K)}{P_{\mathrm{rec}}}}|v|\right), \tag{20}$$

where P_{rec} and K are the parameters of the distribution and I_0 is the modified Bessel function of the first kind and zero order.

The parameter P_{rec} is the *average received power* given by

$$P_{\mathrm{rec}} = \langle |v|^2 \rangle, \tag{21}$$

where $\langle\rangle$ denotes the sample average operation.

The parameter K is the *Ricean $K-$factor* defined as the power ratio of the fixed and fluctuating components, i.e., the power of the dominant path $|v_{\mathrm{s}}|^2$ and the power of all other paths $\langle |v_{\mathrm{d}}|^2 \rangle$

$$K = \frac{|v_{\mathrm{s}}|^2}{\langle |v_{\mathrm{d}}|^2 \rangle}, \tag{22}$$

where $P_{\mathrm{rec}} = |v_{\mathrm{s}}|^2 + \langle |v_{\mathrm{d}}|^2 \rangle$.

It is worthwhile noticing that a crucial question is how to define the reflections of the dominant signal from the other MPS antennas. In the equations introduced in Section II above we have assumed that the AoA of the reflected waves are naturally incorporated as part of the scattering around the dominant signal. Therefore, reflections of the dominant signal will affect the level of the non-dominant signals v_{d}, and that way affect the $K-$factor. However, a different way of looking at it would be to consider the scattered waves to be a part of v_{s} because they might not have independent and random phase relative to the direct signal path. In this case, the differences in path lengths of the scattered signals will affect the level of the dominant path, and thereby affect the $K-$factor. The latter interpretation is left to a future study.

B. Ricean Fading Emulation Accuracy

The impact of scattering within the UCA MPS array on the Ricean fading emulation accuracy is evaluated by looking

upon the distribution parameters (21) and (22). The corresponding measurement uncertainties are the average received power uncertainty[1] and the Ricean $K-$factor uncertainty.

Average received power uncertainty: Consider the ratio between the average received power with and without the scattering component from all the MPS antennas

$$\epsilon_P = \frac{P_{\text{rec}}^{\text{total}}}{P_{\text{rec}}^{\text{direct}}}, \tag{23}$$

where $P_{\text{rec}}^{\text{total}}$ and $P_{\text{rec}}^{\text{direct}}$ are computed applying (21) to (9), (4), (3) and (10), (7), (6), (5), respectively. A closed form expression for ϵ_P can be derived for a uniform 2D distribution of AoA (see Appendix A), it is however not necerary to assume uniform Rayleigh

$$\epsilon_P = 1 + \left(\frac{G\lambda}{8\pi R}\right)^2 \sum_{\ell=1}^{N_{\text{MPS}}-1} \frac{1}{\sin^2\left(\frac{\pi\ell}{N_{\text{MPS}}}\right)}, \tag{24}$$

where G is the antenna gain assumed to be equal for all the MPS antennas and the DUT antenna too, R is the radius of the MPS ring and N_{MPS} is the number of MPS antennas. Here it is also worthwhile noticing that the second term of (24) is the disturbance level introduced in [14]. Clearly, $\epsilon_P \geq 1$ since scattered power will add up to the direct power and $\epsilon_P = 1$ is achieved in case of no scattering effects. The impact of scattering is anticipated to be of the order of 1 dB or less [14].

We define the average receive power uncertainty[2] in dB as follows

$$\delta_P = 20\log 10(1 + \sqrt{\epsilon_P - 1}). \tag{25}$$

where ϵ_P has been defined by (23) and (24). As we can see from (25) $\delta_P = 0$ dB, when there is no unwanted scattered power since $\epsilon_P = 1$. If the unwanted scattered power is present then $\delta_P > 0$ dB which increases with the power ratio ϵ_P. Hence, as the unwanted scattered power increases the uncertainty (25) also increases. As we can see from (24), the uncertainty (25) is the same independently of the $K-$factor as we would expect. (24) is approximately a half of the uncertainty given by (4) in [14] when $\epsilon_P - 1 \ll 1$, which makes a reasonably good agreement between our approaches.

Ricean $K-$factor uncertainty: Similarly to the power uncertainty we start considering the ratio between the $K-$factor with and without the scattering component

$$\epsilon_K = \frac{K^{\text{total}}}{K^{\text{direct}}}, \tag{26}$$

where K^{total} and K^{direct} are computed applying (22) to the corresponding signals as in the average power case computations above. An expression for ϵ_K is derived in terms of the gain of the antennas, radius of the MPS ring and the number of MPS antennas (see Appendix B)

$$\epsilon_K = \frac{1}{1 + \left(1 + \frac{K_{\text{in}} N_{\text{MPS}}}{N_{\text{MPS}}-1}\right)\left(\frac{G\lambda}{8\pi R}\right)^2 \sum_{\ell=1}^{N_{\text{MPS}}-1} \frac{1}{\sin^2\left(\frac{\pi\ell}{N_{\text{MPS}}}\right)}}, \tag{27}$$

where K_{in} is the *input* $K-$factor that corresponds to the Ricean fading statistics we aim to emulate.

It is expected that $\epsilon_K \leq 1$ since the contribution to the non-coherent power component, i.e., $\langle |v_{\text{d}}|^2 \rangle$ in (22) will increase due to scattering and thus, leading to a small $K-$factor. In the case of no scattering we have $\epsilon_K = 1$.

The Ricean $K-$factor uncertainty can be defined in dB as follows

$$\delta_K = 20\log 10(1 + \sqrt{1 - \epsilon_K}). \tag{28}$$

As in the case of the average power uncertainty, the $K-$factor uncertainty $\delta_K = 0$ dB when there is no unwanted scattered power since $\epsilon_K = 1$. An increase of unwanted scattered power results in an increase of δ_K.

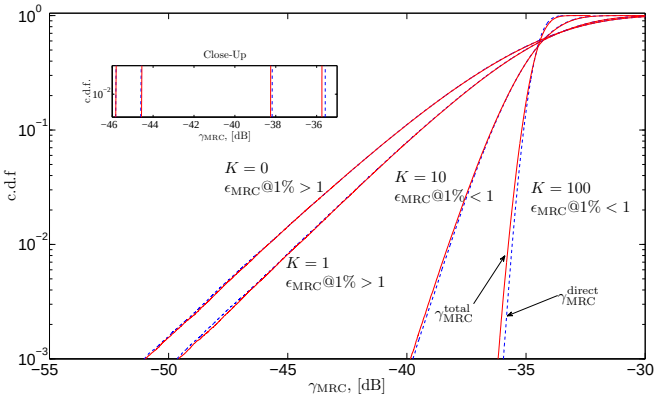

Fig. 2: Cumulative distribution function of the MRC corresponding to direct signals, i.e. without scattering, and signals with the scattering component present.

C. Diversity Combining

Here we study the impact of the scattering on the MRC diversity. It is assumed that the variance of the Additive White Gaussian Noise (AWGN) equals one. Thus, the output of the MRC gives the signal-to-noise ratio, [20]

$$\gamma_{\text{MRC}} = \sum_{n=1}^{N_{\text{DUT}}} |v_n|^2, \tag{29}$$

where v_n are the voltages induced at antenna port n of the DUT and N_{DUT} is the number of antenna ports, i.e., diversity branches.

MRC diversity uncertainty: MRC diversity uncertainty can be defined at different cumulative distribution function (cdf) probability levels of (29). Firstly, let's define the ratio between the average MRC with and without scattering

$$\epsilon_{\text{MRC}} = \frac{\langle \gamma_{\text{MRC}}^{\text{total}} \rangle}{\langle \gamma_{\text{MRC}}^{\text{direct}} \rangle}, \tag{30}$$

where $\gamma_{\text{MRC}}^{\text{total}}$ and $\gamma_{\text{MRC}}^{\text{direct}}$ are given by (29) with v_n replaced by v_n^{total} and v_n^{direct}, respectively. It is expected that $\epsilon_{\text{MRC}} \geq 1$

[1] In practice a change in average power can be taken care of by calibration. However, the uncertainty of the average power for different taps in an impulse response in a wideband system is critical since the average power level might in general be different for each tap.

[2] We have defined the uncertainty to be as a function of $20\log 10(...)$ instead of $10\log 10(...)$ as it's been defined in [14].

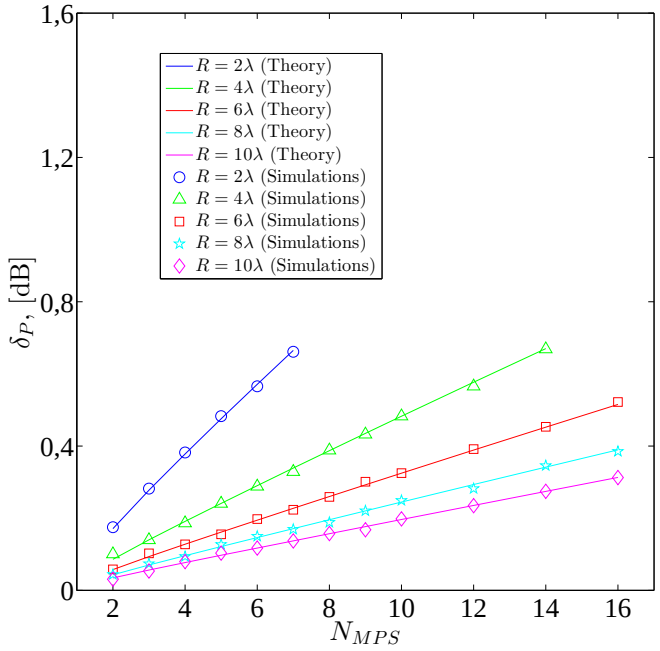

Fig. 3: Average received power uncertainty δ_P [dB] v.s. the number of MPS antennas N_{MPS} for different MPS ring radii R.

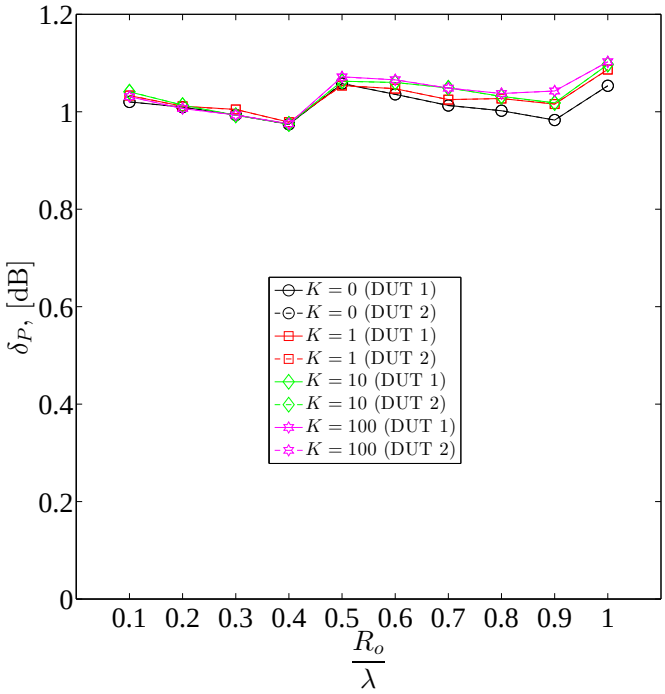

Fig. 4: Average received power uncertainty δ_P [dB] v.s. the normalized separation distance R_o for different Ricean $K-$factors. The two-antenna DUT system is considered with MPS simulation parameters from Table I. DUT1 and DUT2 denote each antenna element in the two-antenna DUT system.

since scattered power will add up to the direct power and $\epsilon_{\text{MRC}} = 1$ is achieved in case of no scattering effects. This can be clearly understood noticing that (30) is the same as

$$\epsilon_{\text{MRC}} = \frac{\sum_{n=1}^{N_{\text{DUT}}} P_{\text{rec},n}^{\text{total}}}{\sum_{n=1}^{N_{\text{DUT}}} P_{\text{rec},n}^{\text{direct}}} = \epsilon_P, \tag{31}$$

for independent identically distributed MRC diversity branches (see (23)). This of course is applicable only when the DUT antennas receive the same signals in average.

Following our approach we can then define the MRC diversity uncertainty in dB as follows

$$\delta_{\text{MRC}} = 20 \log 10(1 + \sqrt{\epsilon_{\text{MRC}} - 1}). \tag{32}$$

In addition to the average level, the MRC diversity gain is commonly defined at some probability level p of the cdf. Hence, we here consider $p = 1\%$ to illustrate the impact of scattering on the distribution of the MRC signal. In this case we define the ratio between the MRC signal with and without scattering corresponding to the $p = 1\%$ as follows

$$\epsilon_{\text{MRC@1\%}} = \frac{\gamma_{\text{MRC}}^{\text{total}}@1\%}{\gamma_{\text{MRC}}^{\text{direct}}@1\%}. \tag{33}$$

The MRC diversity uncertainty evaluated at 1% given in dB is then

$$\delta_{\text{MRC@1\%}} = 20 \log 10(1 + \sqrt{|\epsilon_{\text{MRC@1\%}} - 1|}). \tag{34}$$

Both δ_{MRC} and $\delta_{\text{MRC@1\%}}$ equal 0 dB when the unwanted scattering is not present but increase as the unwanted scattering power increases.

Here, as it can be inferred from Fig. 2 based on simulated data, $\epsilon_{\text{MRC@1\%}}$ may be less or greater than 1 depending on the K factor. In this case, the combined effects of average power increase and $K-$factor reduction in the presence of scattering will result not only in a shift of cdf but also a change of the slope of the MRC signal. As previously, equality to one is obtained when no scattering is present.

V. Numerical Experiments and Analysis

In this section we present an analysis of the uncertainty parameters δ_P, δ_{K}, δ_{MRC} and $\delta_{\text{MRC@1\%}}$ given in Section IV. The uncertainty parameters are evaluated as a function of the number of MPS antennas $N_{\text{MPS}} \in \{2, 16\}$, the normalized radius of the MPS ring $R/\lambda \in \{2, 10\}$ and the Ricean fading parameter $K = \{0, 1, 10, 100\}$. We present numerical experiments based on the scattering model introduced in Section II and the Ricean fading statistics assumption (20)-(22). First, we evaluate the results for each considered parameter by assuming an antenna spacing of $R_o = \lambda/2$. Secondly, in order to characterize the uncertainty of compact UCA MPS OTA systems we consider the separation distance of R_o/λ with corresponding $\min(R/\lambda)$ and $\max(N_{\text{MPS}})$ chosen according to Table I. Two main scenarios are considered regarding the number of DUT antennas, i.e., one-antenna and two-antenna DUT systems comprising vertically polarized half-wavelength dipoles with unit gain, i.e., 0 dBi. The one-antenna DUT is placed in the center of the MPS simulator. In the two-antenna DUT case, the antenna elements are placed symmetrically around the center of the MPS array as shown in Fig. 1. Each simulation point was obtained based on $n = 2 \times 10^6$ independent samples of the fading statistics. In addition, the data is further analyzed

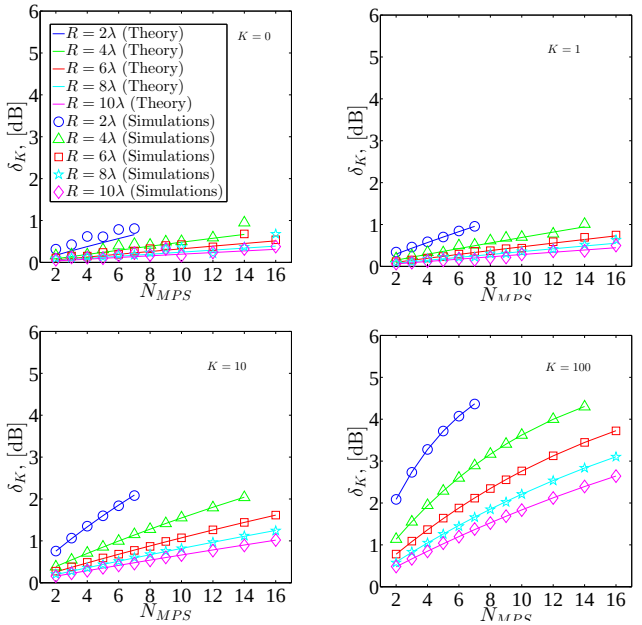

Fig. 5: Ricean $K-$factor uncertainty [dB] v.s. the number of MPS antennas N_{MPS} for different MPS ring radii and different input $K-$factors.

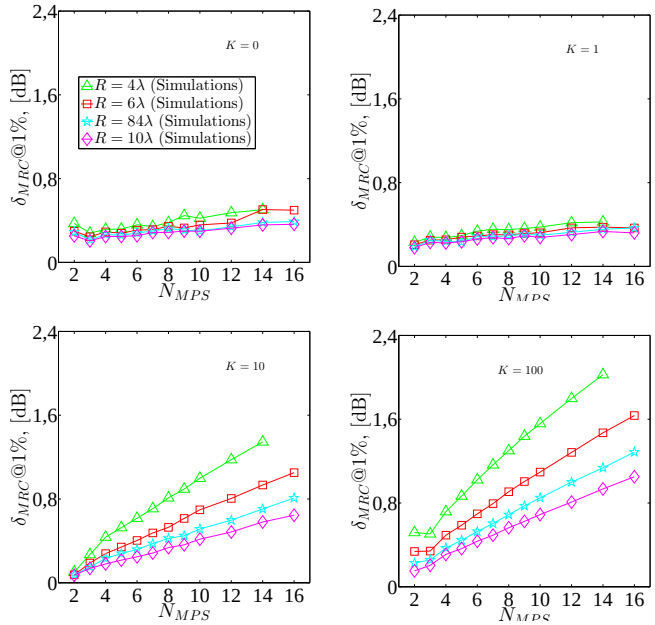

Fig. 7: MRC diversity uncertainty at the 1% probability level δ_{MRC}@1% [dB] v.s. the number of MPS antennas N_{MPS} for different MPS ring radii and different input $K-$factors.

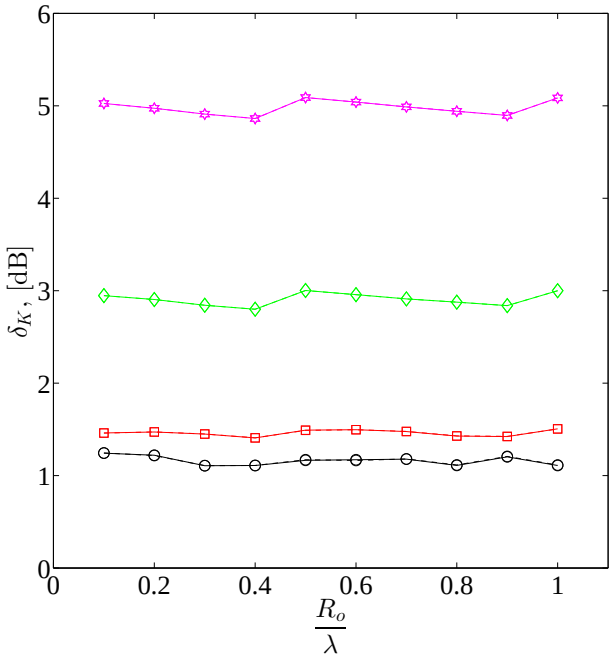

Fig. 6: Ricean $K-$factor uncertainty δ_K [dB] v.s. the normalized separation distance R_o for different Ricean $K-$factors. The two-antenna DUT system is considered with MPS simulation parameters from Table I. For legend see Fig. 4.

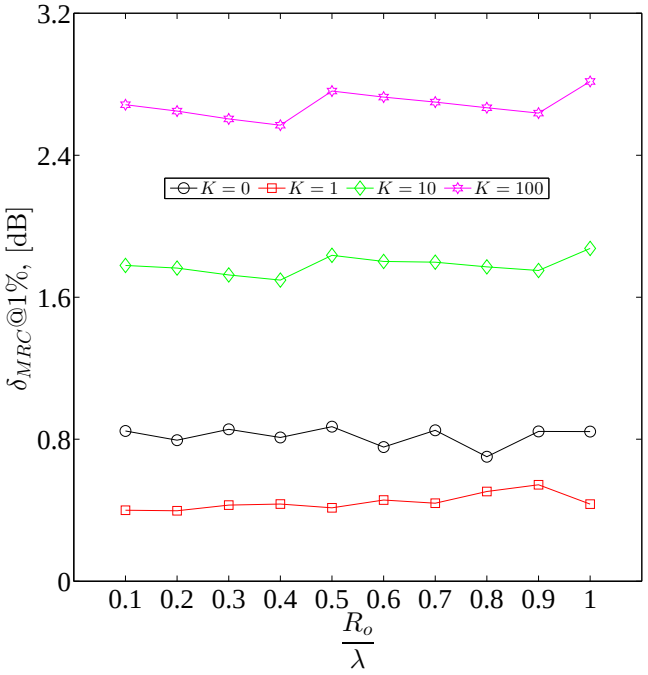

Fig. 8: MRC diversity uncertainty at the 1% probability level δ_{MRC}@1% [dB] v.s. the normalized separation distance R_o for different Ricean $K-$factors. The two-antenna DUT system is considered with MPS simulation parameters from Table I.

by resampling the data with $n = 1 \times 10^6$ data points in a bootstrapping approach [21]. The employed Ricean $K-$factor estimator is based on the method-of-moments described in [22]. We compare simulation results to analytical expressions where applicable.

Since we are interested in investigating the impact of scattering we adopt a simplified Ricean fading model to generate the desired first order statistics. The simulations are based on a UCA MPS antenna arrangement comprising of vertically polarized half-wavelength dipole antennas also with unit gains for the sake of convenience. Each MPS antenna transmits signals of constant amplitudes proportional to the square root

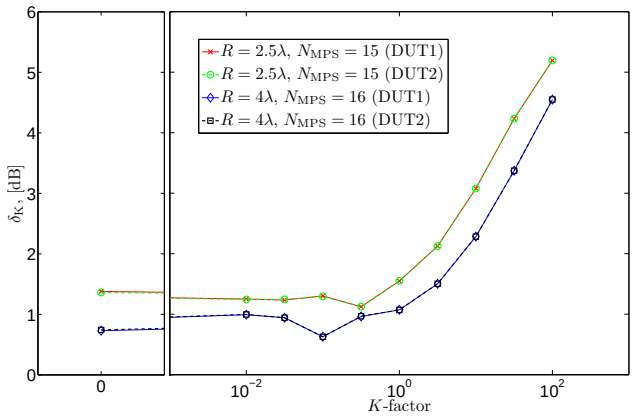

Fig. 9: Ricean $K-$factor uncertainty δ_K [dB] v.s. input Ricean $K-$factors. A two-antenna DUT system is considered with element separation $R_o = \lambda/2$.

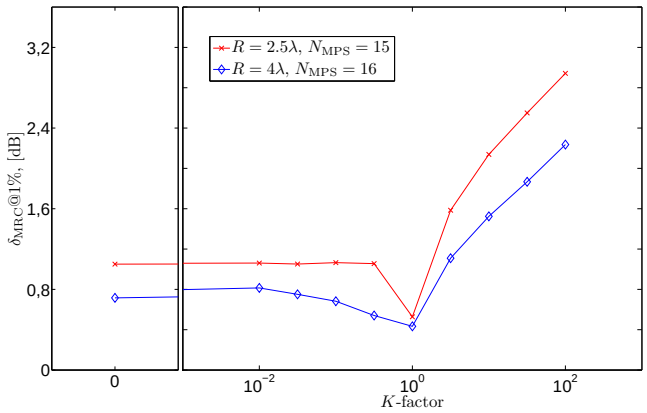

Fig. 10: MRC diversity uncertainty at the 1% probability level $\delta_{\mathrm{MRC}}@1\%$ [dB] v.s. input Ricean $K-$factors. A two-antenna DUT system is considered with element separation $R_o = \lambda/2$.

of the radiated power $\sqrt{P}$. The phases ψ of the transmit signals, on the other hand, are changed randomly between 0 and 2π and drawn from a 1D uniform distribution (i.e., the induced voltages at a DUT antenna $v \sim \sqrt{P}\mathrm{e}^{-j(\psi)}$ as shown in Section II). In order to obtain a Rayleigh distributed signal (i.e., $K = 0$ in (20)), all the amplitudes transmitted by the MPS antennas are assumed to be equal. Thus, in our model we assume for $K = 0$ the input power of MPS antenna m is given by

$$P_m = \frac{1}{N_{\mathrm{MPS}}} \text{ for all } m. \tag{35}$$

The Ricean fading (i.e., $K > 0$ in (20)), is achieved when the amplitude of one of the transmit signals is larger than all the others (see Appendix B and [24] for further details). In this case, the input power of MPS antenna m is given by

$$P_m = \begin{cases} \frac{K_{\mathrm{in}} N_{\mathrm{MPS}}}{K_{\mathrm{in}} N_{\mathrm{MPS}} + N_{\mathrm{MPS}} - 1} & \text{if } m = 1 \\ \frac{1}{K_{\mathrm{in}} N_{\mathrm{MPS}} + N_{\mathrm{MPS}} - 1} & \text{otherwise} \end{cases}, \tag{36}$$

where P_1 is the transmit power by the MPS antenna that simulates the fixed path, while all the other represents the transmit power by the MPS antennas $m \neq 1$ and emulate the fluctuating paths in Ricean fading. As can be seen from

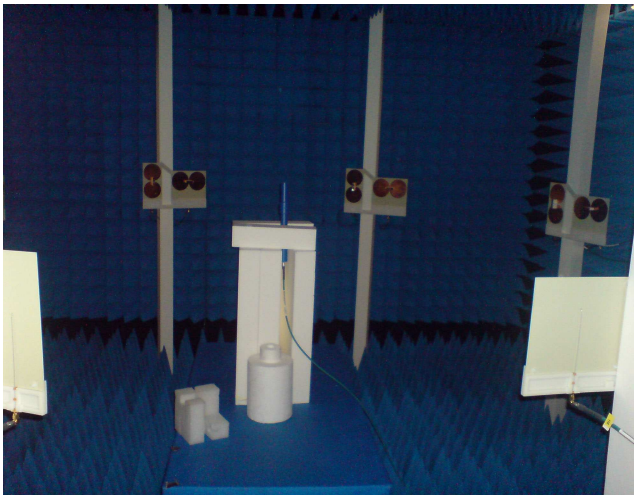

Fig. 11: MPS system in anechoic room with 8 pairs orthogonally polarized MPS antennas. The receiving vertically polarized half-wavelength dipole is shown in the center of the MPS array.

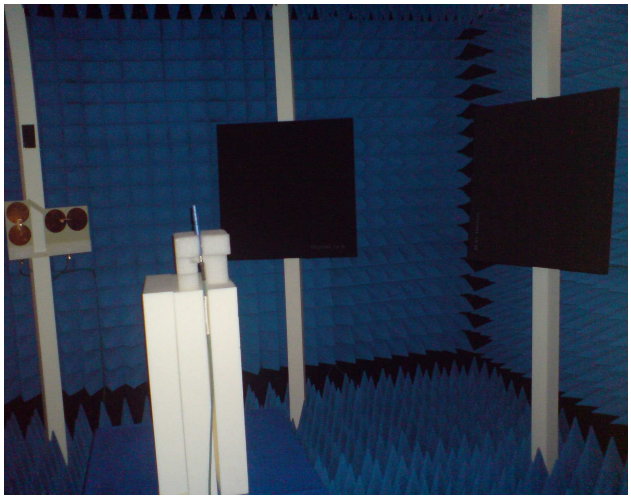

Fig. 12: Same as in Fig.11, but with flat laminate absorbers.

(35) and (36), the total input power to the MPS antennas is normalized to one. It is worthwhile to mention that the signal variation can be modeled by the Ricean distribution with $K = 0$ (i.e., Rayleigh distribution) with good accuracy for $N_{\mathrm{MPS}} \geq 6$, [24]. As K increases, the number of required MPS antennas might be lower.

A. Average Received Power Uncertainty

The results of the average received power uncertainty corresponding to the one-antenna DUT case are shown in Fig. 3. Similar results were obtained for the two-antenna DUT case with antenna element spacing $R_o = 0.5\lambda$ and therefore are omitted. Fig. 3 illustrates the dependence of δ_P upon the number of MPS antennas N_{MPS} for different values of the ring radius to wavelength ratios R/λ. Moreover, the small spread in values correspond to different $K-$factors; δ_P is independent of the Ricean $K-$factor as we had concluded in Section IV above. As we can see from Fig. 3, the impact of scattering increases with the number of MPS antennas, i.e.,

from $N_{\mathrm{MPS}} = 2$ to $N_{\mathrm{MPS}} = 16$, whereas it decreases with the size of the MPS ring radius, i.e., from $R = 2\lambda$ to $R = 10\lambda$. So implementing a UCA MPS OTA system with $N_{\mathrm{MPS}} = 16$ antennas and ring radius $R = 10\lambda$ will result in an average received power uncertainty $\delta_P \approx 0.30$ dB. This result is well in line with the results obtained in [14]. The discrete points represent simulated results, while theoretical results (see (24) and (25)) are shown by the continuous lines.

Fig. 4 shows the average received power uncertainty corresponding to the two-antenna DUT case as a function of the separation distance between the DUT antennas R_o given in wavelengths at $K = 0$, $K = 1$, $K = 10$ and $K = 100$. Furthermore, as we wanted to understand the impact of the limitations of the far-field conditions (18) and (19) on δ_P we produced the results with R/λ and N_{MPS} according to Table I.

As expected, the variations δ_P as a function of $K-$factor are small and are a result of numerical uncertainties. Moreover, we can see from Fig. 4 that δ_P is also rather constant and equals approximately 1 dB in average. The small oscillations we believe are a result of the geometrical disposition of the DUT array within the MPS array. As we can see, $\delta_P = 1$ dB is much higher than most values shown in Fig. 3. This can be explained by the fact that, in the majority of the considered cases, the ring radii were much larger than those in Table I. Clearly, the average received power uncertainty could be reduced by decreasing the number of MPS antennas. Hence, Fig. 4 shows an upper bound on δ_P which is independent of the maximum separation between the DUT antenna elements. In other words, we have obtained the worst case average received power uncertainty for the "miniaturization" of the UCA MPS OTA testing.

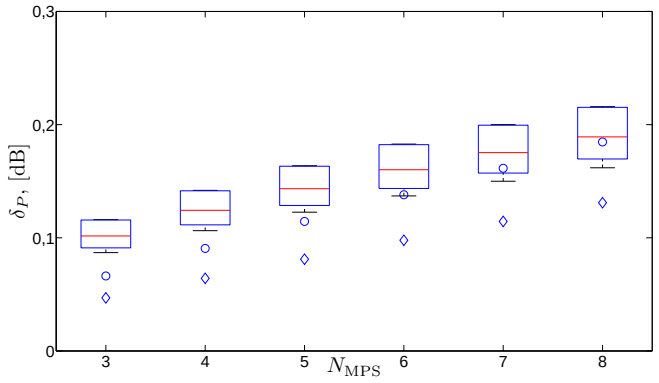

Fig. 13: Average received power uncertainty δ_P [dB] v.s. the number of MPS antennas N_{MPS} at MPS ring radius $R = 12\lambda$. The boxplot correspond to the parameter estimated from measurements. The diamonds and the circles correspond to predictions with our model with the difference that in the latter case (circles) we double the scattered power.

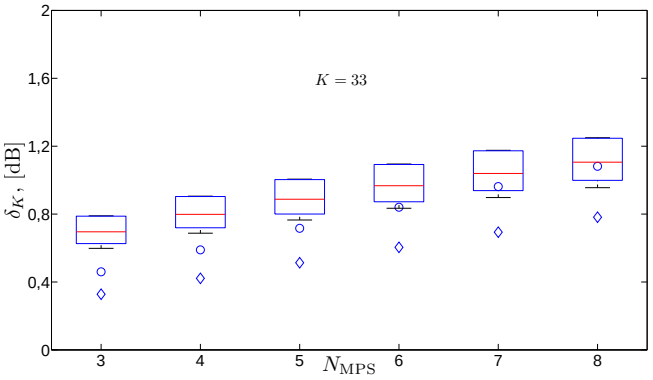

Fig. 14: Ricean $K-$factor uncertainty [dB] v.s. the number of MPS antennas N_{MPS} at MPS ring radius $R = 12\lambda$. The boxplot correspond to the parameter estimated from measurements. The diamonds and the circles correspond to predictions with our model with the difference that in the latter case (circles) we double the scattered power.

B. Ricean $K-$factor uncertainty

Fig. 5 shows the Ricean $K-$factor uncertainty results for the one-antenna DUT case. Here also similar results were obtained for the two-antenna DUT case with antenna element separation $R_o = 0.5\lambda$ and therefore are omitted. As we can see from Fig. 5, δ_K increases with the number of MPS antennas, whereas it decreases with the size of the MPS ring radius. Moreover, δ_K increases with the $K-$factor. This can be understood by noticing the fact that scattering from the MPS array antennas will add power to fluctuating paths but relatively much less to the fixed path component, which causes the $K-$factor to decrease (see (22)). The impact considerably increases for large $K-$factors. The discrete points represent simulated results, while theoretical results (see (27) and (28)) are shown by the continuous lines.

The results in Fig. 6 are plotted in a similar way as described for Fig. 4. The results in Fig. 6 show almost no variation of the Ricean $K-$factor uncertainty as a function of the separation distance between the DUT antennas in an MPS system. On the other hand, the uncertainty considerably increases as a function of the Ricean $K-$factor. It is worthwhile noticing the variation (oscillations) of the uncertainty for $K = 0$, which can be explained by the stochastic nature of the underlying simulation, but also inaccuracies introduced by the employed Ricean $K-$factor estimator at $K = 0$, [22] (see [23] for an alternative estimator). In Fig. 6, it is also observed that results are similar for both the DUTs. Following a similar reasoning as in Fig. 4 we can conclude that plots shown in Fig. 6 represent an upper bound on δ_K which is independent of the maximum separation between the DUT antenna elements.

Fig. 9 shows the dependence of the Ricean $K-$factor uncertainty as a function of the input $K-$factor for two different sets of values of MPS ring radius and number of MPS antennas. As we can see, the uncertainty increases with the $K-$factor for $K \gtrsim 1$, while for lower values, i.e., less than 1, there are small fluctuations. The trend depends on the MPS ring radius and number of MPS antennas.

C. MRC Diversity Uncertainty

In this section, the MRC diversity uncertainty is discussed for both the average power and the power corresponding to

the 1% cdf probability level of the combined signals (29), i.e., δ_{MRC} and $\delta_{\mathrm{MRC}}@1\%$, respectively. The two-antenna DUT system comprises two identical antennas with spacing $R_o = 0.5\lambda$. Then, the average MRC diversity uncertainty is, in this case, equal to the average power uncertainty, i.e., $\delta_{\mathrm{MRC}} = \delta_P$ (see (31)). Hence, for an analysis of the average MRC diversity uncertainty behavior please see Section V.A.

Results for the MRC diversity uncertainty evaluated at the 1% cdf probability level are given in Fig. 7. As we can see, $\delta_{\mathrm{MRC}}@1\%$ increases with the number of MPS antennas, but decreases with the size of the MPS ring radius. Furthermore, the increase of $\delta_{\mathrm{MRC}}@1\%$ with the Ricean $K-$factor can be clearly observed for larger $K-$ factors, but $\delta_{\mathrm{MRC}}@1\%$ is slightly larger at $K = 0$ than for $K = 1$.

Fig. 8 shows the dependence of $\delta_{\mathrm{MRC}}@1\%$ on R_o/λ for different Ricean $K-$factors. Fig. 8 was obtained in a similar way as described above for Fig. 6, Fig. 5 and Fig. 3. Here, $\delta_{\mathrm{MRC}}@1\%$ remains almost constant as a function of the normalized separation distance between the antenna elements R_o and UCA MPS parameters chosen from Table I. On the other hand, at smaller $K-$factors, i.e., $K = 0$ and $K = 1$, $\delta_{\mathrm{MRC}}@1\%$ oscillates due to the stochastic nature of the simulations. Here, the uncertainty at $K = 0$ is larger than at $K = 1$. This can be explained by the impact of scattering on the MRC signal, which depends on the $K-$factor as shown in Fig. 2. For $K = 0$, we have that $\epsilon_{\mathrm{MRC@1\%}} > 1$, but decreases with the increase of $K-$factor. For $K \approx 1$ and above $\epsilon_{\mathrm{MRC@1\%}} < 1$, but the uncertainty (34) increases since $|\epsilon_{\mathrm{MRC@1\%}} - 1|$ increases even faster leading to a minimum for $K = 1$ as illustrated in Fig. 10.

VI. Experimental Validation

Above, we studied a large number of different performance measures under various MPS system parameters both numerically and analytically. In this section we present the experimental evaluation of the average received power uncertainty δ_P and the Ricean $K-$factor uncertainty δ_K. For this purpose we use the MPS system at the Sony Mobile Communications facility in Lund, Sweden. The MPS system comprises 16 identical omnidirectional UWB antennas with a scattering parasitic element. 8 antennas are horizontally polarized and the other 8 are vertically polarized as shown in Fig.11. Hence, up to 16 different signal paths can be simulated. Different Doppler spectra can be simulated by feeding the MPS antennas via a sweeping phase shifter. The amplitude of each path can be controlled by attenuators fed to the MPS antennas. A vector network analyzer is used to record the complex transmission coefficient S_{21} between the antenna under test (AUT) and the MPS antennas. Further information can be found in [25].

To estimate the impact of scattering we specialize our investigations to the vertically polarized case and therefor only up to 8 paths were generated since $N_{MPS} = 8$ in our case. The CW (Continuous Wave) measurements were performed at the LTE-A band of 2600 MHz with a vertically polarized half-wavelength antenna placed in the center of the MPS system. The MPS ring radius was fixed and equal to 1.4 m, which at 2600 MHz gives $R = 12\lambda$. For our purposes we din't use the phase shifter.

The experimental procedure is described next. We started by covering all the MPS antenna pairs but one with flat laminate absorbers as shown in Fig.12. The average reflection coefficient of the absorbers is -20 dB over the considered frequency band. We then collected a sequence of 16001 values of S_{21}. In order to emulate a given $K-$factor value, i.e., 0, 5 and 33, we repeated the measurements with three different transmit powers, i.e., the power to one of the MPS antennas is varied, while keeping the other powers fixed. This procedure was repeated 6 times to check for consistency. Next, we removed a second absorber, a third and so on until all eight absorbers were removed. Each time we collected the same amount of data, i.e., we have 8 sets of $16001 \times 3 \times 6$ values of S_{21}.

We reduce the effect of the additive white gaussian noise by averaging over the 16001 points which improves the signal to noise ratio by 42 dB and reduces the data to 3×6 vectors containing 8 elements each. Then we minimize the squared error norm between the complex measured signals and the model in Section II. This leads to a nonlinear optimization problem, which we solve numerically by means of the fmincon Interior Point Algorithm implemented in the Matlab Optimization Toolbox [26]. Among the set of solutions we have chosen the data with the lowest fitting errors between measurement and model. The data with large fitting errors give also large measurement uncertainties. We assume they are not caused by scattering within the MPS system.

The obtained results are shown in Fig.13 and Fig.14; they depict the average received power uncertainty δ_P and the Ricean $K-$unceratinty δ_K for $K = 33$ (results for $K = 0$ and $K = 5$ follow a similar trend but with lower values). The boxplots show the statistics of the estimated uncertainties. The circles and the diamonds represent the results obtained from the model when the scattered power is accounted for twice or only once, respectively. As we can see, the agreement between data and model is rather good, especially for the case when scattered power in the model is doubled (given by the circles). This is explained by the fact that our model considers only one ring of MPS antennas, while the used MPS system comprises two superimposed rings, one of them with passive antennas. Moreover, we see that the disagreement increases as we move towards the lower values of N_{MPS}. This difference can be explained by the fact that with fewer N_{MPS} antennas the contribution from the adjacent (orthogonally polarized passive antenna) has a larger relative contribution to the scattering as compared to the case with a larger number of MPS antennas.

VII. Discussion & Conclusions

The study of the impact of scattering within an MPS array on the measurement uncertainty is evaluated for a narrowband Ricean channel by performing MPS simulations based on the proposed MPS scattering model and the derived far-field criteria. Based on the simulation results it can be said that the average received power uncertainty, the Ricean $K-$factor uncertainty and the MRC diversity uncertainty (both average and at the 1 % probability level), they all increase with the larger number of MPS antennas and decrease with the smaller

radius of the MPS ring. Typical values of the number of MPS antennas and radii of the MPS ring are within $8-16$ and $2-10$ wavelengths, respectively. In this case it was found that the average received power uncertainty is within $0.1-0.7$ dB. The Ricean $K-$factor uncertainties for $K=0$ and $K=10$ are within $0.1-1$ dB and $0.5-2$ dB, respectively. The corresponding MRC diversity uncertainties at the 1 % probability level are within $0.2-0.6$ dB and $0.3-1.5$ dB for $K=0$ and $K=10$, respectively.

The general trend is that uncertainty also increase with the Ricean $K-$factor except for the average power uncertainty and the average MRC diversity uncertainty which are shown not to depend on the $K-$factor. Thus, the obtained results suggest that to counter the impact of the scattering within the MPS antennas emulating a Ricean fading environment one has to design a large MPS system and this leads to higher costs.

To keep costs low we therefore need to "miniaturize" the UCA MPS system while keeping measurement uncertainties at an acceptable levels. We have shown that if the UCA MPS system fulfills the derived far-field criteria, then there is a certain minimum ring radius and a maximum number MPS antennas for each maximum separation between antennas in a DUT system. Under these conditions, the considered uncertainties change only slightly as a function of the maximum separation between antennas in a DUT system.

Future studies could consider the combined impact of reflections from the chamber walls and reflections from the MPS array. Other aspect of interest could be study cross-talk within the measurement equipment, which may set an upper limit to the $K-$factor that can be implemented.

ACKNOWLEDGEMENTS

We would like to thank the anonymous reviewers for their insightful comments and suggestions that have contributed to improve our paper.

Parts of the research leading to these results have received funding from the European Research Council under the European Community's Seventh Framework Programme (FP7/2007-2013) / ERC grant agreement no. 228044.

The authors would like to thank Juan Diego Sanchez Heredia for his expert help during the measurement campaign at SonyMobile Communications site in Lund.

APPENDIX A: DERIVATION OF THE AVERAGE RECEIVED POWER UNCERTAINTY

Let's assume a UCA MPS system with N_{MPS} MPS antennas and one DUT antenna which are co-polarized (i.e., $\eta=1$ in (3)) and have equal gain G as in the case of omnidirectional antennas. According to Section II the total power received at a DUT is the sum of the direct and the indirect powers

$$P^{\mathrm{total}}=P^{\mathrm{direct}}+P^{\mathrm{indirect}}, \tag{37}$$

where the total direct power is given by

$$P^{\mathrm{direct}}=\sum_{m=1}^{N_{\mathrm{MPS}}}P_m^{\mathrm{direct}}, \tag{38}$$

and the total indirect (i.e., scattered) power is given by

$$P^{\mathrm{indirect}}=\sum_{m=1}^{N_{\mathrm{MPS}}}\sum_{\ell\neq m}^{N_{\mathrm{MPS}}}P_{\ell,m}^{\mathrm{indirect}}. \tag{39}$$

The direct receive power at the DUT arriving from the fed MPS antenna m with transmit power P_m can be written as follows according to Friis transmission formula (3)

$$P_m^{\mathrm{direct}}=P_m\left(\frac{G\lambda}{4\pi R}\right)^2. \tag{40}$$

The indirect receive power at the DUT which has been scattered by passive MPS antenna ℓ, but radiated by fed MPS antenna m is obtained by combining (5) and (6)

$$P_{\ell,m}^{\mathrm{indirect}}=P_m\left(\frac{G\lambda}{4\pi R}\right)^2\left(\frac{G\lambda}{4\pi R_{\ell,m}}\right)^2, \tag{41}$$

where $R_{\ell,m}$ is the distance between MPS antenna m and MPS antenna ℓ which for a UCA MPS system is given by

$$R_{\ell,m}=2R\sin\left(\frac{\pi|\ell-m|}{N_{\mathrm{MPS}}}\right). \tag{42}$$

Now substituting (41) into (39) gives

$$P^{\mathrm{indirect}}=\sum_{m=1}^{N_{\mathrm{MPS}}}P_m\left(\frac{G\lambda}{4\pi R}\right)^2\sum_{\ell=1}^{N_{\mathrm{MPS}}-1}\left(\frac{G\lambda}{4\pi R_\ell}\right)^2, \tag{43}$$

where due to circular symmetry

$$R_{\ell,m}=R_\ell=2R\sin\left(\frac{\pi\ell}{N_{\mathrm{MPS}}}\right). \tag{44}$$

Combining the above equations and substituting the result in (23) gives the sought result for the average received power uncertainty (24).

APPENDIX B: DERIVATION OF THE RICEAN $K-$FACTOR UNCERTAINTY

The Ricean $K-$factor of the direct signal, i.e., without scattering is defined as

$$K^{\mathrm{direct}}=\frac{P_{\mathrm{s}}^{\mathrm{direct}}}{P_{\mathrm{d}}^{\mathrm{direct}}}. \tag{45}$$

where by applying the model given by (35) and (36) together with results presented in Appendix A we obtain the direct power for the fixed component and the Ricean $K-$factor K_{in}

$$P_{\mathrm{s}}^{\mathrm{direct}}=\frac{K_{\mathrm{in}}N_{\mathrm{MPS}}}{K_{\mathrm{in}}N_{\mathrm{MPS}}+N_{\mathrm{MPS}}-1}\left(\frac{G\lambda}{4\pi R}\right)^2. \tag{46}$$

The direct power due to the fluctuating $N_{\mathrm{MPS}}-1$ paths is written as follows

$$P_{\mathrm{d}}^{\mathrm{direct}}=\frac{N_{\mathrm{MPS}}-1}{K_{\mathrm{in}}N_{\mathrm{MPS}}+N_{\mathrm{MPS}}-1}\left(\frac{G\lambda}{4\pi R}\right)^2. \tag{47}$$

Now by substituting (46) and (47) in (45) we obtain

$$K^{\mathrm{direct}}=\frac{K_{\mathrm{in}}N_{\mathrm{MPS}}}{N_{\mathrm{MPS}}-1}. \tag{48}$$

The Ricean $K-$factor of the total power is by definition

$$K^{\mathrm{total}}=\frac{P_{\mathrm{s}}^{\mathrm{total}}}{P_{\mathrm{d}}^{\mathrm{total}}}, \tag{49}$$

where the total and the direct power of the fixed component are equal, i.e., $P_{\rm s}^{\rm total} = P_{\rm s}^{\rm direct}$, as a result of the scattering model in Section II.

The total power due to the fluctuating $N_{\rm MPS}-1$ paths and Ricean $K-$factor $K_{\rm in}$ can be written as

$$P_{\rm d}^{\rm total} = \frac{N_{\rm MPS}-1}{K_{\rm in}N_{\rm MPS}+N_{\rm MPS}-1}\left(\frac{G\lambda}{4\pi R}\right)^2 A + \frac{K_{\rm in}N_{\rm MPS}}{K_{\rm in}N_{\rm MPS}+N_{\rm MPS}-1}\left(\frac{G\lambda}{4\pi R}\right)^2 B, \quad (50)$$

where

$$B = \sum_{\ell=1}^{N_{\rm MPS}-1}\left(\frac{G\lambda}{4\pi R_\ell}\right)^2, \quad (51)$$

and $A = 1 + B$. By substituting (50) and (46) in (49) we obtain

$$K^{\rm total} = \frac{K_{\rm in}N_{\rm MPS}}{(N_{\rm MPS}-1)\,A + K_{\rm in}N_{\rm MPS}B}. \quad (52)$$

Now (52) can be further simplified and written as follows:

$$K^{\rm total} = \frac{K_{\rm in}N_{\rm MPS}}{(N_{\rm MPS}-1) + (K_{\rm in}N_{\rm MPS}+N_{\rm MPS}-1)\,B}. \quad (53)$$

The $K-$factor uncertainty (27) is then obtained by straightforward algebraic substitutions that are omitted due to lack of space. Substituting (44) into (51) and further substituting the obtained result into (53) gives an expression for $K^{\rm total}$. We can now substitute the resulting expression and (48) into (26) that readily leads to (27).

REFERENCES

[1] A. F. Molisch, *Wireless Communications*, Second Edition: John Wiley & Sons, New York, 2011.

[2] CTIA Certification, Test Plan for Mobile Station Over the Air Performance, "Method of Measurement for Radiated RF Power and Receiver Performance," Revision Number 3.1, January 2011.

[3] 3GPP TS 34.114 V11.1.0 (2012-06), "User equipment (UE) / mobile station (MS) over the air (OTA) antenna performance"; Conformance testing (Release 11).

[4] European Cooperation in Science and Technology Action IC1004, "Cooperative Radio Communications for Green Smart Environments," http://www.ic1004.org/.

[5] A. Alayón Glazunov, V. M. Kolmonen and T. A. Laitinen. Chapter 15 "MIMO Over-the-Air Testing" in *LTE-Advanced and Next Generation Wireless Networks - Channel Modelling and Propagation*, John Wiley & Sons, October 2012.

[6] 3GPP TR 37.976 V11.0.0 (2012-03), "Measurement of radiated performance for Multiple Input Multiple Output (MIMO) and multi-antenna reception for High Speed Packet Access (HSPA) and LTE terminals" (Release 11)

[7] M. Rumney, R. Pirkl, M. H. Landmann, and D. A. Sanchez-Hernandez, "MIMO Over-The-Air Research, Development, and Testing," *International Journal of Antennas and Propagation*, vol. 2012, Article ID 467695, 8 pages, 2012. doi:10.1155/2012/467695

[8] G. F. Pedersen, M. Pelosi, J. Welinder, T. Jamsa, A. Yamamoto, M. Nurkkala, S. L. Ling, W. Schroeder and T. Brown, "OTA Test Methods for Multi Antenna Terminals," Chapter 5, COST2100 Final Report, Springer, 2012.

[9] T. Sakata, A. Yamamoto, H. Iwai, K. Ogawa, J.-I. Takada, K. Sakaguchi, and K. Araki, "BER evaluation system for a handset antenna in a multipath environment using a spatial fading emulator," in Proc. ISAP, Seoul, Korea, 2005, pp. 351354.

[10] W. A. T. Kotterman, M. Landmann, A. Heuberger and R. S. Thoma, "New laboratory for Over-The-Air testing and Wave Field Synthesis," General Assembly and Scientific Symposium, XXXth URSI, Aug.13-20, 2011.

[11] P. Hallbjörner, Z. Ying, M. Håkansson, C. Wingqvist, T. Anttila, and J. Welinder, "Multipath simulator for mobile terminal antenna characterisation," *Microw., Antennas Propag.*, vol. 4, no. 6, pp. 743-750, 2010.

[12] A. Khatun, T. Laitinen, V-M. Kolmonen, and P. Vainikainen, "Dependence of Error Level on the Number of Probes in Over-the-Air Multiprobe Test Systems," *International Journal of Antennas and Propagation*, vol. 2012, 6 pages, 2012.

[13] P. Kyösti and L. Hentilä, "Criteria for physical dimensions of MIMO OTA multi-probe test setup, in Proceedings of the 6th European Conference on Antennas and Propagation (EuCAP'12), Prague, Czech Republic, March 2012.

[14] P. Hallbjörner, "Measurement Uncertainty in Multipath Simulators Due to Scattering Within the Antenna Array-Theoretical Model Based on Mutual Coupling," *IEEE Antennas and Wireless Propag. Letters*, vol. 9, pp.1103-1106, 2010.

[15] I. Kim, S. Xu and Y. Rahmat-Samii, "Generalised correction to the friis formula: quick determination of the coupling in the fresnel region," Microwaves, Antennas & Propagation, IET , vol.7, no.13, pp.1092,1101, October 22, 2013, doi: 10.1049/iet-map.2013.0131.

[16] S. Silver, *Microwave Antenna Theory and Design*, Third Edition: Peter Peregrinus Ltd., on behalf of IEE, London, UK, 1997.

[17] C. A. Balanis, *Antenna Theory, Analysis and Design*, Second Edition: John Wiley & Sons, Inc., New York, 1997.

[18] W. C. Jakes Jr., *Microwave Mobile Communications,* John Willey & Sons Interscience, 1974.

[19] T. M. Cover, J. A. Thomas, *Elements of Information Theory*, John Wiley & Sons, New York, NY, 1991.

[20] J. B. Andersen, "Antenna Arrays in Mobile Communications-Gain, Diversity and Channel Capacity," Radio Science Bulletin, vol. 290, pp.4-7, 1999.

[21] A. C. Davison, D. V. Hinkley, *Bootstrap Methods and their Application*, Cambridge University Press, New York, NY, 1997.

[22] L. J. Greenstein, D. G. Michelson and V. Erceg, "Moment-Method Estimation of Ricean K-factor," *IEEE Communications Letters*, vol. 3, no.6, June 1999.

[23] P. Händel, S. Prasad, C. Beckman, "Maximum likelihood estimation of reverberation chamber direct-to-scattered ratio," *Electronics Letters*, Vol. 45, No. 25, December 2009.

[24] M. Pätzold, *Mobile Fading Channels*, John Wiley & Sons, Chichester, UK, 2002.

[25] P. Hallbjörner, J.D. Sanchez-Heredia, P. Lindberg, A.M. Martinez-Gonzalez, T. Bolin, "Multipath Simulator Measurements of Handset Dual Antenna Performance With Limited Number of Signal Paths," Antennas and Propagation, IEEE Transactions on, vol.60, no.2, pp.682-688, Feb. 2012.

[26] MATLAB Optimization Toolbox.
[online]. Avaialble: http://www.mathworks.se/help/optim/ug/fmincon.html

Andrés Alayón Glazunov (SM'−2011) was born in Havana, Cuba, in 1969. He obtained the M.Sc. (Engineer-Researcher) degree in Physical Engineering from Saint Petersburg State Polytechnical University, Russia, and the Ph.D. degree in Electrical Engineering from Lund University, Sweden, during 1988 − 1994 and 2006 − 2009, respectively. From 1996 to 2001, he was a member of the Research Staff at Ericsson Research, Ericsson AB in Kista, Sweden, where he conducted research in the areas of advanced receiver performance evaluation for UMTS, applied electromagnetic wave propagation and stochastic channel modelling for wireless communications systems. During this period he also contributed to the European COST Action 259 project in the directional channel modelling working group. In 2001, Alayón Glazunov joined Telia Research, Sweden, as a Senior Research Engineer. Later, starting 2003, he held a position as a Senior Specialist in Antenna Systems and Propagation at the newly formed TeliaSonera Sweden, where he pursued research in smart antennas and MIMO, network optimization and Over-The-Air (OTA) performance evaluation of handsets and their impact on wireless network performance. From 2001 to 2005 he was the Swedish delegate to the European COST Action 273 and was active in the handset antenna working group. He has been one of the pioneers in establishing OTA measurement techniques. He has contributed to the EVEREST and NEWCOM European research projects as well as to the 3GPP and the ITU standardization bodies. During 2009 and 2010, Alayón Glazunov held a Marie Curie Senior Research Fellowship at the Centre for Wireless Network Design (CWiND), University of Bedfordshire, UK. Currently, he is a post-doc at the Electromagnetic Engineering Lab, KTH-The Royal Institute of Technology, Stockholm, Sweden.

Andrés Alayón Glazunov is the author of numerous scientific and technical publications. He is the co-author and co-editor of LTE-Advanced and Next Generation Wireless Networks (Wiley 2012). His current research interests include, but are not limited to, statistical signal processing, electromagnetic theory, fundamental limitations on antenna-channel interactions, RF propagation channel measurements, modelling and simulations for network optimization, and OTA testing of wireless devices.

Sathyaveer Prasad was born in Hyderabad, India. He received Bachelor of Technology degree in Electronics and Communications engineering with distinction from Jawaharlal Nehru Technological University (JNTU), Hyderabad, India in 2000. He completed his Master of Science degree in Electronics and Telecommunications engineering from University of Gävle, Sweden in 2005. He received his Licentiate of Engineering and PhD degree in Telecommunications from Royal Institute of Technology (KTH), Stockholm, Sweden in 2011 and 2013, respectively. Before starting his doctoral studies at KTH and University of Gävle, Sweden in 2007 he had the opportunity to work at TeliaSonera AB, Sweden and Siemens Space Business group, Czech Republic and Austria. Currently, he is self-employed at Prasad Consulting Services, Gävle, Sweden. His research interests are antennas and wave propagation, antenna measurements and antenna design for mobile communications.

Peter Händel (S'88−M'94−SM'98) received the Ph.D. degree from Uppsala University, Uppsala, Sweden, in 1993. He was with Uppsala University from 1987 to 1993. From 1993 to 1997, he was with Ericsson AB, Kista, Sweden. From 1996 to 1997, he was with the Tampere University of Technology, Tampere, Finland. Since 1997, he has been with the Royal Institute of Technology, Stockholm, Sweden, where he is currently a Professor of signal processing and Head of the Department of Signal Processing. Dr. Händel has served as a member of the Editorial Board of the Journal on Advances in Signal Processing, as a member of the Editorial Advisory Board of Recent Patents on Electrical Engineering, and as an Associate Editor for IEEE TRANSACTIONS ON SIGNAL PROCESSING.

Thomas Bolin MSc AP & EE LiTH 1979. Industry background: RF-Engineer at ITT Standard Radio & Telefon AB in Stockholm 1979 − 1983 in R&D of maritime kW HF-transmitters, technical manager at Ericsson and Sony Ericson in Lund in 1985 − 2009 in mobile phone RF and Antenna Design. Present position: Master Engineer at the Network Technology Research Lab of Sony Mobile Lund with a responsibility of terminal MIMO antenna design and measurement technology. Is a member of the Sony Mobile IPR-board. Holds some 10 patents and is co-author to a few scientific papers.

Kjell Prytz received his BSc in physics and his PhD in high energy physics in 1984 and 1991, respectively, both from Uppsala University. In 1998 he was appointed Docent in high energy physics at Uppsala University. He has worked at CERN and DESY laboratories in high energy physics and has since 1996 been employed as lecturer in physics at Gävle University College, Sweden.